

AN AMBIGUITY FUNCTION SYNTHESIS APPROACH TO DESIGNING ORTHOGONAL WAVEFORMS FOR SPACE SURVEILLANCE

Giorgio de Moura Magalhães and Martin Käske

Fraunhofer Institute for High Frequency Physics and Radar Techniques FHR, Fraunhoferstr. 20, 53343 Wachtberg, Germany, Email: {giorgio.de.moura.magalhaes, martin.kaeske}@fhr.fraunhofer.de

ABSTRACT

The effective separation of radar signals from multiple transmitter stations is vital for accurate detection and tracking of objects in Space Situational Awareness (SSA). In this paper, we address the problem of jointly designing transmitting waveforms and receiving filters to produce a set of Auto-Ambiguity Functions (AAF) and Cross-Ambiguity Functions (CAF) with orthogonal properties. While doing so, we also consider the challenges of coherently integrating multiple pulses affected by the high radial velocities and accelerations of space objects. The proposed approach employs the Ambiguity Function Synthesis methodology, which provides flexibility in both choosing a desired shape for the AAF and CAF and optimizing for orthogonality in a specific region. We conduct numerical experiments to demonstrate the effectiveness of the synthesized waveforms and compare their performance against classical sequences and state-of-the-art methods in terms of Peak Sidelobe Level (PSL) and Averaged Sidelobe Level (ASL).

Keywords: Ambiguity Function Synthesis; Orthogonal Waveform Design; CDMA; Space Surveillance.

1. INTRODUCTION

A network of radar sensors serves as an effective system for space debris monitoring, providing increased coverage, detection sensitivity, and tracking accuracy in Space Situational Awareness (SSA). In a radar network operating in MIMO mode, a receiver must be able to distinguish between signals originating from different transmitters, as the delay of each signal, together with the position of the respective transmitter, is crucial for determining the position of the target. Take, for example, the configuration shown in Figure 1. The receiver will sense two echoes arriving from Tx1 and Tx2 and will be able to measure the distance they traveled from their respective echo delay. With a correct distinction regarding which echo comes from which transmitter, the ellipses in continuous lines are determined, and their intersection represents the correct target position. On the other hand, if

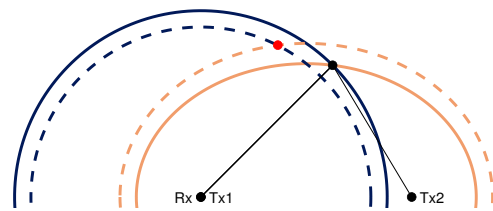


Figure 1. Target position estimation dependency on transmitter position.

the association is mixed, the dashed ellipses are found instead, leading to a wrong estimation of the target position.

The problem of distinguishing transmitters can be solved by adapting methods developed for telecommunications that are used for multiple access. These methods are based on spatial division, time division, frequency division, code division, or a combination of some of these techniques [1]. In addition to these methods, a division in the Doppler domain can also be found in the literature [2]. The limitations of some of these methods, however, make their application for radar networks less attractive. First, spatial separation is not possible, as the signals between the target and the receiver must use the same spatial channel. Second, time division is not resource-efficient, as all transmitters, except one, would be idle during each transmission. Third, it is also not feasible to divide the signals into frequency bands, as this could significantly increase the required bandwidth with an increasing number of transmitters. Fourth, a division in the Doppler domain imposes conflicting requirements on the maximum unambiguous range/Doppler and PRF.

Therefore, we focused on asynchronous Code-Division Multiple Access (CDMA) methods applied to radar waveforms. Each transmitter is assigned a different code, and their waveforms are modulated with the corresponding code before transmission. The receiver can use the coded waveform of a specific transmitter to recover its respective signal. The signals from other transmitters are considered interference to be suppressed. The challenge is to find a set of codes that are orthogonal to each other so that the waveform of one transmitter is suppressed when processed with the filter matched to any other transmitter. The main disadvantage of CDMA methods lies in the po-

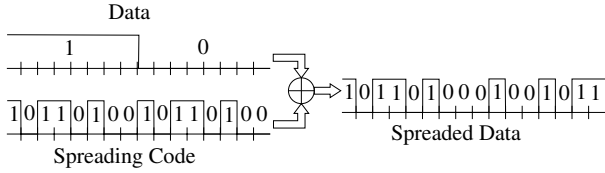


Figure 2. Schematic concept of DSSS techniques.

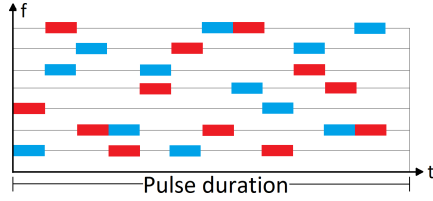


Figure 3. Schematic concept of FHSS techniques.

tentially high range/Doppler sidelobes [2], which highly depend on the chosen codes. Therefore, when searching for a suitable set of orthogonal codes, one should consider not only the cross-correlation properties (orthogonality) but also the auto-correlation properties (sidelobes).

CDMA is based on the Spread Spectrum (SS) technique, where the transmitted waveform is intentionally spread in frequency and occupies a higher bandwidth than the required minimum. This is achieved through an spreading signal. SS techniques are classified into two main groups: Direct Sequence Spread Spectrum (DSSS) and Frequency Hopping Spread Spectrum (FHSS). Figures 2 and 3 show a simplified schematic representation of the concepts of FHSS and DSSS. In DSSS, the waveform is directly multiplied by the spreading code signal. At the receiver, the spreaded signal is correlated by a synchronized copy of the coded waveform, which reverses the spreading (despreading). In FHSS, different frequency shifts are consecutively applied to pieces of the original waveform. The frequency shift (hop) pattern is different for each transmitter, even though all transmitters share the same total bandwidth when the whole pulse duration is considered. With good choices of code, conflicts between the transmitters can be minimized even in the presence of time delays and frequency shifts. A hybrid approach is also possible and is exploited in this work.

The CDMA scheme can be applied to radar systems in Slow-Time or Fast-Time. In Fast-Time CDMA, each pulse is individually spread, and orthogonality is to be achieved pulse by pulse, while in Slow-Time CDMA one code chip is used per pulse and orthogonality is achieved only after integrating the pulses. In Fast-Time CDMA, the bandwidth is influenced by the chip duration, and the sidelobes can increase depending on the chosen code. On the other hand, the signal processing is basically the same, so there is no additional computational burden. In Slow-Time CDMA, the sidelobes and bandwidth remain unaffected, as only a constant phase/frequency shift is applied per pulse. However, the Doppler sidelobes can be high depending on the code. Additionally, orthogonality can be affected by the target Doppler frequency, as it

is determined only after the coherent sum of the pulses. This requires a joint range-Doppler processing, which can increase the system's computational load [2]. It is also possible to apply both Slow- and Fast-Time CDMA, that is, every pulse in a train of pulses is multiplied by different code sequences. At reception, they are individually processed in fast-time, and the result is integrated in slow time. One reason for doing so is that this allows for exploring the so-called Complementary Codes.

A set of Complementary Codes presents the property that the sum of their individual auto-correlation functions presents the ideal impulse shape, as their sidelobes cancel each other out. An example of such code set is the Golay sequence pair [3]. Although the Golay pair presents an ideal auto-correlation function, the property of zero cross-correlation with another sequence is not fulfilled. Therefore, it does not constitute an orthogonal set. The Complete Complementary Codes (CCC), on the other hand, are a class of codes that possesses ideal auto- and cross-correlation functions [4]. An example of such code sets is explored in [5], where the authors investigate multiple CCC with Zero Cross-Correlation Zone (ZCCZ). However, the sidelobe cancellation occurs only for zero Doppler speed offset. For some non-zero Doppler speed values, the sidelobes can be quite high, inducing ambiguities. This reinforces that, one must evaluate the shapes of both the auto-correlation functions of all waveforms and the cross-correlation functions for every pair of waveforms, considering not only zero but also reasonable non-zero Doppler speeds. On a positive note, we see that the usage of different codes for the multiple pulses can provide cancellation of sidelobes and improve orthogonality properties after pulse integration.

The use of different codes for each pulse is also motivated by the possibility of avoiding the constant volume property of the Ambiguity Functions [6, 7, 8]. The pulses are processed independently by different filters, and the outputs are coherently integrated. Since the sum of Ambiguity Functions is not an Ambiguity Function, except when the waveforms are the same [6], the sum of the filter outputs will no longer obey to the constant volume property. In fact, consider that P pulses $x_p(t) \in L^2(\mathbb{R})$ are transmitted, each with normalized energy $\|x_p\|_{L^2(\mathbb{R})} = 1$, the volume under the sum of their ambiguity functions $A_p \in L^2(\mathbb{R}^2)$ is given by

$$\left\| \sum_{p=0}^{P-1} A_p \right\|_{L^2(\mathbb{R}^2)} = \sum_{p=0}^{P-1} \|A_p\|_{L^2(\mathbb{R}^2)} = P \|x_p\|_{L^2(\mathbb{R})}^2 = P \quad (1)$$

The first equality comes from the orthogonality (in slow-time) of the pulses, while the second comes from Moyal's identity $\|A_{uv}\|_{L^2(\mathbb{R}^2)} = \|x_u\|_{L^2(\mathbb{R})} \|x_v\|_{L^2(\mathbb{R})}$. If one would transmit a single pulse $x \in L^2(\mathbb{R})$ with equivalent total energy $\|x\|_{L^2(\mathbb{R})} = P$, the volume under its Ambiguity Function would be $\|A\|_{L^2(\mathbb{R}^2)} = \|x\|_{L^2(\mathbb{R})}^2 = P^2$. That is, we observe a reduction in a factor of P in the volume property, indicating a potential sidelobe level reduction since the peak at the main lobe is equal to P in both cases. Ultimately, there is only one signal being trans-

mitted, spread over a long time period, and the constant volume property of the Ambiguity Function is still valid for the train of pulses as a waveform. The use of complementary waveforms is merely a device to manipulate the Ambiguity Function by pushing the lobes into less harmful parts of the range-Doppler plane [6, 9].

Codes for CDMA can be obtained in different ways. The deterministically defined codes are generated by straightforward, well-defined procedures. These codes, such as Walsh-Hadamard, M-Sequence, Gold, Kasami, and Costas, are predictable and easier to implement. Walsh-Hadamard codes are mutually orthogonal binary codes popular for synchronous CDMA applications. Reference [10] utilized them in radar signal modulation to enhance resilience against electronic countermeasures, though their orthogonality properties were not exploited. Reference [11] evaluated their auto- and cross-correlation properties, noting that some codes in a Hadamard matrix had ideal cross-correlation, while others showed high sidelobes. The primary issue was that their auto-correlation functions had many high sidelobes, making them unsuitable for asynchronous cases. Maximum Length Sequences (MLS), or M-Sequences, are binary pseudorandom sequences constructed from primitive polynomials defining an n -stage feedback shift register [12]. M-Sequences exhibit quasi-orthogonal auto-correlation functions with a value of 1 at zero delay and $-1/N$ for other time shifts. Their cross-correlation functions do not follow a pattern [13], but some properties can be derived [14]. Reference [12] compares M-Sequences with LFM waveforms for delay and Doppler shift estimation. Gold and Kasami sequences are derived from M-Sequences [13]. Gold codes, formed from the modulo-2 sum of two different M-Sequences, have bounded cross-correlation values, while Kasami codes are constructed from even M-Sequences and are optimal concerning the Welch bound. The Costas code is utilized for FHSS waveforms, forming a frequency hop pattern with at most one chip out-of-phase coincidence for delayed and frequency-shifted versions. The properties of two Costas arrays' cross-correlation depend on the construction method. An issue with the Costas code is to find a large set of codes with good cross-correlation properties, limiting the number of transmitters [15]. Additionally, the literature includes polyphase codes for DSSS, such as Frank, FZC, and Oppermann codes, evaluated in [16]. For FHSS, a chaos-based pseudo noise sequence was also found, with average auto- and cross-correlation properties calculated [17].

The codes can also be obtained through optimization algorithms that enhance specific performance criteria. Heuristic and metaheuristic methods yield acceptable results quickly through trial and error, though they do not guarantee optimality [18]. Over 500 new metaheuristic algorithms have been developed as of 2023 [18]. This variety of algorithms is also evident in methods specifically aimed at generating sets of orthogonal codes. A common characteristic is using auto and cross-correlation functions to define fitness functions, combining Peak Sidelobe Level (PSL) and Integrated Sidelobe Level (ISL). Most

studies focus on single-pulse designs using Polyphase DSSS with optimization algorithms like Simulated Annealing [19, 20], Cross Entropy [21], and Genetic Algorithms [22, 23]. Some works apply single-pulse FHSS [24, 25] or combine DSSS and FHSS [26, 27]. The study [28] explores multiple pulses for DSSS using the Adam optimizer with a convolutional neural network. Several studies incorporate additional modulation techniques such as the Linear Frequency Modulation (LFM) [29, 26, 27]. While [19, 28] consider Doppler effects, most papers optimize solely for 0-Doppler conditions, limiting their applicability in dynamic environments. However, studies [21, 20, 29, 27] evaluate Doppler tolerance after optimization. In summary, despite the exploration of various optimization algorithms for orthogonal waveform design, significant gaps remain in addressing Doppler shift implications, crucial for effective space applications.

Deterministic iterative methods, in contrast to heuristic and metaheuristic approaches, produce codes through defined, repeatable processes that systematically refine them. These methods, however, have limited exploration capabilities, often converging to local minima and struggling with high-dimensional code optimization problems. Metaheuristic methods can provide initial guesses for these deterministic methods, potentially enhancing their convergence and performance. The literature on deterministic iterative methods for orthogonal waveform design includes both single-pulse and complementary multiple-pulse configurations, primarily focusing on Polyphase DSSS techniques. Studies optimizing single-pulse codes employ methods such as Cyclic Algorithms (CAN, WeCAN, CAD) [30], quasi-Newton method L-BFGS [31], Sequential Cone Programming [32], Iterative Sequential Quartic Optimization [33], manifold-based algorithms [34], and majorization-minimization (MM) techniques combined with coordinate descent [35] or the alternating direction method of multipliers (ADMM) [36]. Most focus on 0-Doppler conditions and use objective functions based on auto-correlation and cross-correlation metrics. Notable exceptions [32, 35, 36] consider Doppler effects during optimization and analyze their impact on performance. While single-pulse algorithms can be adapted to multi-pulse configurations, one must account the effect of Doppler on phase after the Pulse Repetition Interval, and range migration and acceleration cannot be neglected. Regarding complementary multiple pulses, the study [37] addresses multi-sequence optimization using a Majorization-Minimization algorithm but only considers a set of complementary sequences (ideal auto-correlation after summation) or orthogonal codes (single pulse). The optimization of sets of complementary codes with orthogonal properties is not addressed, and they optimize solely for 0-Doppler conditions.

This paper proposes a deterministic iterative method based on the Cross-Ambiguity Function (CAF) synthesis technique from [38], considering multiple pulses with complementary codes and the effects of high velocities and acceleration present in Space Situational Awareness (SSA). The problem of synthesizing the CAF involves

calculating the transmitting waveform and receiving filter that yield a CAF approximating a desired function across all time and Doppler offsets within a specified region [38, 39, 7]. In these studies, both the waveform and receiver filter are modeled as a sequence of adjacent pulses weighted by a complex code. The CAF is computed as a function of the transmitting and receiving codes, and an objective function is defined to assess how closely the obtained CAF approximates the target CAF. The core challenge lies in determining the code that optimizes this objective function. The optimization problem is solved interactively, fixing some parameters while obtaining others by setting the gradient to zero. The work in [8] also addresses Ambiguity Function synthesis and proposes a computationally faster algorithm, but it considers only the thumbtack Ambiguity Function. None of these works account for the orthogonality of multiple waveforms. In this study, we utilize a Generalized Ambiguity Function (GAF) that considers target parameters instead of constant delay and frequency shift. The developed method allows for different codes for multiple pulses, aiming to exploit sidelobe cancellation by summing ambiguity functions, as is the case for Complete Complementary Codes (CCC), and to avoid the constant volume property of the Ambiguity Function, which implies that reducing sidelobes in one region necessitates increasing them in another [6, 7]. Moreover, the synthesis approach offers simplicity and flexibility, allowing us to approximate the Ambiguity Function to a desired shape depending on the application. For instance, in a tracking task where an estimate of the target parameters is available, one can optimize for a smaller region around the expected target, neglecting other regions to achieve potentially better orthogonality in the area of interest.

This paper is organized as follows: Section 2 presents the signal model; Section 3 develops an expression for the Ambiguity Function of the spread spectrum waveforms; Section 4 analyzes the SNR loss due to the use of an unmatched filter; Section 5 formulates the waveform optimization problem; Section 6 develops the solution; Section 7 provides numerical results; and Section 8 concludes the paper.

2. SIGNAL MODEL

Let $\tilde{x}_u^{\text{tx}}(t) = \Re\{x_u^{\text{tx}}(t)e^{j2\pi f_c t}\}$ be the signal from the u -th transmitter, where $x_u^{\text{tx}}(t)$ is the baseband signal and f_c is the carrier frequency. The received signal is approximately proportional to the delayed transmitted waveform, $\tilde{x}_u^{\text{tx}}(t - \tau(t; \theta))$, where $\tau(t; \theta)$ is a time-dependent delay parameterized by the target parameters θ . After demodulation in the receivers, the echo originated from the u -th transmitter is:

$$x_u(t; \theta) = x_u^{\text{tx}}(t - \tau(t; \theta))e^{-j2\pi f_c \tau(t; \theta)} \quad (2)$$

The considered baseband waveform $x_u^{\text{tx}}(t)$ is a train of P pulses, with a Pulse Repetition Interval (PRI) of T_r .

Each pulse, with duration T , is a Spread Spectrum radar waveform, either FHSS or DSSS, described as a sequence of N adjacent rectangular chips of duration $T_c = T/N$, multiplied by a code-dependent function. Explicitly, we write:

$$x_u^{\text{tx}}(t) = \sum_{p=0}^{P-1} x_{up}(t - pT_r) \quad (3)$$

$$x_{up}(t) = \sum_{n=0}^{N-1} a_{upn} e^{j2\pi \alpha_{upn} t} \Pi\left(\frac{t - nT_c}{T_c}\right) \quad (4)$$

where $\Pi(t)$ is the rectangular pulse of unit width starting at $t = 0$. The sequence of unimodular complex numbers $\{a_{upn}\}_{u,p,n \in \mathbb{N}}$ is determined by the phase code (DSSS) and the sequence of real numbers $\{\alpha_{upn}\}_{u,p,n \in \mathbb{N}}$ is determined by the frequency hop code (FHSS).

The filters $y_v(t; \theta)$ employed by the receiver have the same form of $x_u(t; \theta)$ in Equations 2-4, and, in general, are designed to individually filter the signal from the v -th transmitter. The only difference is that we can possibly employ other DSSS and FHSS codes. That is, instead of Equation 4, we write

$$y_{vp}(t) = \sum_{m=0}^{N-1} b_{vpm} e^{j2\pi \beta_{vpm} t} \Pi\left(\frac{t - mT_c}{T_c}\right) \quad (5)$$

and x is correspondingly replaced by y in Equations 2 and 3.

3. AMBIGUITY FUNCTION OF A SPREAD SPECTRUM RADAR WAVEFORM

The conventional tool for analyzing a waveform, considering time and Doppler mismatches with the filter, is the Auto Ambiguity Function (AAF). It is useful for investigating resolution, sidelobe behavior, and ambiguities, both in range and Doppler [40]. To assess the quality of orthogonality, we consider the Cross Ambiguity Function (CAF), which is nothing more than the Ambiguity Function when one waveform is processed with the filter associated to another waveform. A possible mathematical definition of the CAF is

$$C_{uv}(\tau, f) = \int_{-\infty}^{\infty} x_u(t) y_v^*(t - \tau) \exp(-j2\pi f t) dt \quad (6)$$

where τ is the time offset relative to the expected delay, and f is the Doppler mismatch between the true Doppler frequency and the frequency expected by the matched filter.

However, when multiple pulses are coherently integrated, not only the delay and Doppler shift may not be constant over all pulses, but also the effect of acceleration may not be negligible. Equation 6 cannot be directly used, as τ and f are not independent of t . Instead, we use the Generalized Auto- and Cross-Ambiguity Functions [41] defined as the time correlation between the received signal

affected by the true target parameters and a filter tuned to the estimated parameters, as follows:

$$C_{uv}(\boldsymbol{\theta}^*, \boldsymbol{\theta}) = \int_{-\infty}^{\infty} x_u(t; \boldsymbol{\theta}^*) y_v^*(t; \boldsymbol{\theta}) dt \quad (7)$$

where x_u is the echo received from the u -th transmitter, y_v is the filter matched to the v -th transmitter, and $\boldsymbol{\theta}$ is a vector containing target kinematic parameters. The arguments $(\boldsymbol{\theta}^*, \boldsymbol{\theta})$ will occasionally be suppressed throughout the paper for the sake of notation simplification.

We take range (ρ_0), radial speed ($\dot{\rho}_0$), and range acceleration ($\ddot{\rho}_0$) at a reference time t_0 as target parameters, that is, $\boldsymbol{\theta} = [\rho_0 \dot{\rho}_0 \ddot{\rho}_0]^T$. The superscripted star is added to indicate the true values. Notice that, under the assumptions of constant delay and Doppler shift in x_u and y_v , the Generalized Ambiguity Function depends only on the difference in delay and Doppler caused by $\boldsymbol{\theta}^*$ and $\boldsymbol{\theta}$, and Equation 7 reduces to Equation 6, except for a phase factor.

To consider the used Spread Spectrum waveform, we substitute Equation 2 and the corresponding filter $y_v^x(t)$ into Equation 7. We assume that the difference between $\tau(t; \boldsymbol{\theta})$ and $\tau(t; \boldsymbol{\theta}^*)$ is such that different pulses do not intersect for any t . We change the integration variable t by $t_f = t - pT_r$ and evaluate the correlation for each pulse individually in fast time. We neglect fast time changes in τ for the envelopes x_{up} and y_{vp} . Finally, we apply the constant acceleration model $\tau(t; \boldsymbol{\theta}) = \frac{1}{c}\rho(t) = \frac{1}{c}[\rho_0 + \dot{\rho}_0(t - t_0) + \frac{1}{2}\ddot{\rho}_0(t - t_0)^2]$, which also implies that τ depends linearly on $\boldsymbol{\theta} = [\rho_0 \dot{\rho}_0 \ddot{\rho}_0]^T$. The CAF becomes:

$$C_{uv}(\boldsymbol{\theta}^*, \boldsymbol{\theta}) = \sum_{p=0}^{P-1} e^{j2\pi f_c \tau_p(\Delta\boldsymbol{\theta})} C_{uv}^p(\boldsymbol{\theta}^*, \boldsymbol{\theta}) \quad (8)$$

where $\Delta\boldsymbol{\theta} = \boldsymbol{\theta} - \boldsymbol{\theta}^*$,

$$C_{uv}^p(\boldsymbol{\theta}^*, \boldsymbol{\theta}) = \int_{-\infty}^{\infty} x_{up}(t - \tau_p(\boldsymbol{\theta}^*)) y_{vp}^*(t - \tau_p(\boldsymbol{\theta})) e^{j2\pi\nu_p(\Delta\boldsymbol{\theta})t} e^{j\pi\gamma_p(\Delta\boldsymbol{\theta})t^2} dt \quad (9)$$

$\tau_p(\boldsymbol{\theta}) = \tau(pT_r; \boldsymbol{\theta})$ is the echo delay, $\nu_p(\boldsymbol{\theta}) = f_c \dot{\tau}(pT_r; \boldsymbol{\theta})$ is the Doppler frequency, and $\gamma_p(\boldsymbol{\theta}) = f_c \ddot{\tau}(pT_r; \boldsymbol{\theta})$ is the rate of change of the Doppler frequency.

Notice that C_{uv}^p is the CAF of the individual pulses. Considering the pulses form presented in Equations 4 and 5. The CAF between the pulses becomes

$$C_{uv}^p(\boldsymbol{\theta}^*, \boldsymbol{\theta}) = \sum_{n,m=0}^{N-1} a_{upn} b_{vpm}^* C_{uv}^{pnm}(\boldsymbol{\theta}^*, \boldsymbol{\theta}) e^{-j2\pi[\alpha_{upn}\tau_p(\boldsymbol{\theta}^*) - \beta_{vpm}\tau_p(\boldsymbol{\theta})]} \quad (10)$$

where C_{uv}^{pnm} is the CAF between chips and is calculated as

$$C_{uv}^{pnm}(\boldsymbol{\theta}^*, \boldsymbol{\theta}) = \int_{-\infty}^{\infty} \Pi\left(\frac{t - \tau_p(\boldsymbol{\theta}^*) - nT_c}{T_c}\right) \Pi\left(\frac{t - \tau_p(\boldsymbol{\theta}) - mT_c}{T_c}\right) e^{j2\pi[(\alpha_{upn} - \beta_{vpm}) + \nu_p(\Delta\boldsymbol{\theta})]t} e^{j\pi\gamma_p(\Delta\boldsymbol{\theta})t^2} dt \quad (11)$$

To solve this integral, we exploit the fact that it will assume nonzero values if, and only if, the argument of both Π functions is inside the interval $(0, 1)$. A consequence is that $n - m$ can only be $z_p(\Delta\boldsymbol{\theta})$ or $z_p(\Delta\boldsymbol{\theta}) + 1$, where $z_p(\boldsymbol{\theta}) = \left\lfloor \frac{\tau_p(\boldsymbol{\theta})}{T_c} \right\rfloor \in \mathbb{Z}$. Replacing the integral result into the CAF of a pulse (Equation 10) and the result back into Equation 8, we finally obtain the CAF of a Spread Spectrum Radar Waveform:

$$C_{uv} = \sum_{p=0}^{P-1} \sum_{m=0}^{N-1} \sum_{n=m+z_p(\Delta\boldsymbol{\theta})+1}^{m+z_p(\Delta\boldsymbol{\theta})+1} a_{upn} b_{vpm}^* e^{j\Psi_{uv}^{pnm}} X_{uv}^{pnm} \quad (12)$$

where

$$\Psi_{uv}^{pnm} = 2\pi \left[f_c \tau_p(\Delta\boldsymbol{\theta}) - \alpha_{upn} \tau_p(\boldsymbol{\theta}^*) + \beta_{vpm} \tau_p(\boldsymbol{\theta}) + \mathcal{F} t_m - \frac{\gamma_p(\Delta\boldsymbol{\theta}) t_m^2}{2} \right]$$

$$X_{uv}^{pnm} = T_c \Lambda\left(\frac{\mathcal{T}}{T_c}\right) \text{sinc}\left(\mathcal{F} T_c \Lambda\left(\frac{\mathcal{T}}{T_c}\right)\right)$$

$$\mathcal{T} = \tau_p(\Delta\boldsymbol{\theta}) - (n - m)T_c$$

$$\mathcal{F} = \alpha_{upn} - \beta_{vpm} + \nu_p(\Delta\boldsymbol{\theta}) + \gamma_p(\Delta\boldsymbol{\theta}) t_m$$

$$t_m = \frac{\tau_p(\boldsymbol{\theta} + \boldsymbol{\theta}^*) + (n + m + 1)T_c}{2}$$

$$\Lambda(x) := \max(1 - |x|, 0)$$

$$\text{sinc}(x) := \frac{\sin(\pi x)}{\pi x}$$

Equation 12 can be written in a matrix form as

$$C_{uv} = \sum_{p=0}^{P-1} \mathbf{b}_{vp}^H A_{uv}^p(\boldsymbol{\theta}^*, \boldsymbol{\theta}) \mathbf{a}_{up} = \mathbf{b}_v^H A_{uv}(\boldsymbol{\theta}^*, \boldsymbol{\theta}) \mathbf{a}_u \quad (13)$$

where

$$\mathbf{a}_{up} = [a_{up0} \quad a_{up1} \quad \cdots \quad a_{up,N-1}]^T$$

$$\mathbf{b}_{vp} = [b_{vp0} \quad b_{vp1} \quad \cdots \quad b_{vp,N-1}]^T$$

$$[A_{uv}^p]_{mn} = \begin{cases} e^{j\Psi_{uv}^{pnm}} X_{uv}^{pnm} & , n - m = z_p(\Delta\boldsymbol{\theta}) \\ & , n - m = z_p(\Delta\boldsymbol{\theta}) + 1 \\ 0 & , \text{otherwise} \end{cases}$$

$$\mathbf{a}_u = [\mathbf{a}_{u0}^T \quad \mathbf{a}_{u1}^T \quad \cdots \quad \mathbf{a}_{u,P-1}^T]^T$$

$$\mathbf{b}_v = [\mathbf{b}_{v0}^T \quad \mathbf{b}_{v1}^T \quad \cdots \quad \mathbf{b}_{v,P-1}^T]^T$$

$$A_{uv} = \text{diag}(A_{uv}^0, A_{uv}^1, \cdots, A_{uv}^{P-1})$$

4. SNR LOSS DUE TO UNMATCHED FILTER

In the development of an expression for the Ambiguity Function of a Spread Spectrum Radar Waveform, we used a filter with the same form as the transmitted waveform but with possibly different phase and frequency codes (Equations 4 and Equation 5). This choice brings the flexibility of selecting a set of filters that improve the waveforms' orthogonality by allowing a mismatched filter. This comes at a cost of a loss in the SNR since the matched filter is optimal in this sense.

Let the noise $w(t)$ be modeled by a complex-valued additive white Gaussian noise (AWGN) with zero mean and autocorrelation given by $E[w(t)w^*(t')] = \sigma^2\delta(t-t')$. From Equation 7, the noise at the output of the v -th receiver filter is given by

$$W_v(\boldsymbol{\theta}) = \int_{-\infty}^{\infty} w(t)y_v^*(t; \boldsymbol{\theta})dt \quad (14)$$

Replacing the filter model and making the same assumptions made for C_{uv} , we obtain:

$$W_v(\boldsymbol{\theta}) \approx \sum_{p=0}^{P-1} \sum_{m=0}^{N-1} b_{vpm}^* e^{j\Psi_v^{pm}} W_v^{pm} \quad (15)$$

where

$$\Psi_v^{pm} = 2\pi \left[(f_c + \beta_{vpm})\tau_p(\boldsymbol{\theta}) + \mathcal{F}t_m - \frac{\gamma_p(\boldsymbol{\theta})t_m^2}{2} \right]$$

$$W_v^{pm} = \int_{-\frac{T_c}{2}}^{\frac{T_c}{2}} w(t + t_m + pT_r) e^{j2\pi\mathcal{F}t} dt$$

$$\mathcal{F} = \nu_p(\boldsymbol{\theta}) - \beta_{vpm} + \gamma_p(\boldsymbol{\theta})t_m$$

$$t_m = \tau_p(\boldsymbol{\theta}) + mT_c + \frac{T_c}{2}$$

Notice that $E[W_v^{pm}] = 0$ and $E[(W_v^{pm})(W_v^{qn})^*] = \sigma^2 T_c \delta_{pq} \delta_{mn}$. Therefore, $E[W_v] = 0$ and $E[W_v W_v^*] = \sigma^2 T_c \mathbf{b}_v^H \mathbf{b}_v$.

We conclude that the noise power after the receiver filter is $P_N = E[W_v W_v^*] = \sigma^2 T_c \mathbf{b}_v^H \mathbf{b}_v$. The signal power at the correct target parameter vector is given by the amplitude squared of C_{vv} , that is, $P_S = |C_{vv}(\boldsymbol{\theta}^*, \boldsymbol{\theta}^*)|^2 = T_c^2 |\mathbf{b}_v^H \mathbf{a}_v|^2$. Therefore, the Signal-to-Noise Ratio is given by

$$\text{SNR} = \frac{P_S}{P_N} = \frac{T_c}{\sigma^2} \frac{|\mathbf{b}_v^H \mathbf{a}_v|^2}{\mathbf{b}_v^H \mathbf{b}_v} \quad (16)$$

The maximum SNR is achieved by the matched filter $\mathbf{b}_v = \mathbf{a}_v$, so that the SNR loss can be defined as the following ratio

$$L_v = \frac{\text{SNR}_{\max}}{\text{SNR}} = \frac{(\mathbf{a}_v^H \mathbf{a}_v)(\mathbf{b}_v^H \mathbf{b}_v)}{|\mathbf{b}_v^H \mathbf{a}_v|^2} \geq 1 \quad (17)$$

5. PROBLEM FORMULATION

Consider M transmitters. We wish to find a set of M orthogonal waveforms $x_u(t)$ and M receiver filters $y_u(t)$ that can recover the respective waveform while suppressing the others, for $u \in [0, M-1] \subset \mathbb{Z}$. Within the CAF synthesis approach, this means to synthesize M^2 CAF, namely, C_{uv} for $(u, v) \in [0, M-1] \times [0, M-1]$.

Let \hat{C}_{uv} be the desired amplitude of the CAF C_{uv} . We define the synthesis objective function S as

$$S = \sum_{u,v=0}^{M-1} \int_{-\infty}^{\infty} w_{uv} \left| \hat{C}_{uv} e^{j\Psi_{uv}} - C_{uv} \right|^2 d\boldsymbol{\theta} \quad (18)$$

where $w_{uv} = w_{uv}(\boldsymbol{\theta}^*, \boldsymbol{\theta})$ is a weight function that can be used to select the synthesis region, and $\Psi_{uv} = \Psi_{uv}(\boldsymbol{\theta}^*, \boldsymbol{\theta})$ is a phase term introduced to avoid dealing with the absolute value of the CAF. It's easy to see that the minimizer Ψ_{uv} is given by $\Psi_{uv} = \arg\{C_{uv}\}$.

We replace C_{uv} from Equation 13 into Equation 18 and discard the constant term as it does not affect the minimization solution. The objective function is written below as a function of the phase codes:

$$S(\mathbf{a}, \mathbf{b}) = \sum_{u,v=0}^{M-1} \int_{-\infty}^{\infty} w_{uv} \left[|\mathbf{b}_v^H A_{uv} \mathbf{a}_u|^2 - \mathbf{b}_v^H \hat{C}_{uv}^* e^{-j\Psi_{uv}} A_{uv} \mathbf{a}_u - \mathbf{a}_u^H \hat{C}_{uv} e^{j\Psi_{uv}} A_{uv}^H \mathbf{b}_v \right] d\boldsymbol{\theta} \quad (19)$$

where $\mathbf{a} = [\mathbf{a}_0^T \quad \mathbf{a}_1^T \quad \cdots \quad \mathbf{a}_{M-1}^T]^T$ and $\mathbf{b} = [\mathbf{b}_0^T \quad \mathbf{b}_1^T \quad \cdots \quad \mathbf{b}_{M-1}^T]^T$.

By minimizing $S(\mathbf{a}, \mathbf{b})$ we can approximate the Auto- and Cross-Ambiguity Functions to the desired \hat{C}_{uv} functions. However, the SNR loss due to the unmatched filter is not taken into account and could reach excessively high values. To avoid high SNR loss, we additionally define the following objective function to minimize SNR loss.

$$L(\mathbf{a}, \mathbf{b}) = \sum_{u=0}^{M-1} |PN e^{j\Psi_u} - \mathbf{b}_u^H \mathbf{a}_u|^2 - M(PN)^2$$

$$= \sum_{u=0}^{M-1} \left[|\mathbf{b}_u^H \mathbf{a}_u|^2 - PN e^{-j\Psi_u} \mathbf{b}_u^H \mathbf{a}_u - PN e^{j\Psi_u} \mathbf{a}_u^H \mathbf{b}_u \right] \quad (20)$$

where we considered, without loss of generalization, that \mathbf{b}_u^H and \mathbf{a}_u are normalized such that $\mathbf{b}_u^H \mathbf{b}_u = \mathbf{a}_u^H \mathbf{a}_u = PN$. Moreover, $\Psi_u = \arg \{ \mathbf{b}_u^H \mathbf{a}_u \}$ is an auxiliary phase term. Notice that $L(\mathbf{a}, \mathbf{b}) \geq 0$ with the equality being achieved if, and only if, $\mathbf{b}_u = \mathbf{a}_u$, that is, with the matched filter.

The combined objective function is defined as a sum of Equation 18 and Equation 20, weighted by a parameter $\epsilon \in [0, 1]$. The minimization problem is posed as

$$\begin{aligned} \min_{\mathbf{a}, \mathbf{b}} \quad & \Gamma(\mathbf{a}, \mathbf{b}) = \epsilon S(\mathbf{a}, \mathbf{b}) + (1 - \epsilon)L(\mathbf{a}, \mathbf{b}) \quad (21) \\ \text{s.t.} \quad & |a_{upn}| = 1 \quad \text{for } u = 0, 1, \dots, M-1 \\ & \mathbf{b}_{up}^H \mathbf{b}_{up} = N \quad p = 0, 1, \dots, P-1 \\ & n = 0, 1, \dots, N-1 \end{aligned}$$

6. ITERATIVE SOLUTION

Equation 21 constitutes a quartic optimization problem with non-convex constraints and is not easily solved directly. Therefore, we apply the Block Coordinate Descent approach [42], in which the overall optimization is partitioned into simpler sub-problems to be solved in iterative steps: first we assume that \mathbf{b} is constant and optimize for \mathbf{a} , then we do the opposite and consider \mathbf{a} constant to optimize for \mathbf{b} . The objective function for \mathbf{b} and \mathbf{a} fixed becomes, respectively:

$$\mathbf{b} \text{ fixed: } \Gamma(\mathbf{a}) = \mathbf{a}^H F \mathbf{a} - \mathbf{b}^H H \mathbf{a} - \mathbf{a}^H H^H \mathbf{b} \quad (22)$$

$$\mathbf{a} \text{ fixed: } \Gamma(\mathbf{b}) = \mathbf{b}^H G \mathbf{b} - \mathbf{b}^H H \mathbf{a} - \mathbf{a}^H H^H \mathbf{b} \quad (23)$$

where

$$\begin{aligned} F_u &= \epsilon \sum_{v=0}^{M-1} \int_{-\infty}^{\infty} w_{uv} A_{uv}^H \mathbf{b}_v \mathbf{b}_v^H A_{uv} d\boldsymbol{\theta} + (1 - \epsilon) \mathbf{b}_u \mathbf{b}_u^H \\ F &= \text{diag}(F_0, F_1, \dots, F_{M-1}) \\ G_v &= \epsilon \sum_{u=0}^{M-1} \int_{-\infty}^{\infty} w_{uv} A_{uv} \mathbf{a}_u \mathbf{a}_u^H A_{uv}^H d\boldsymbol{\theta} + (1 - \epsilon) \mathbf{a}_v \mathbf{a}_v^H \\ G &= \text{diag}(G_0, G_1, \dots, G_{M-1}) \\ H_{vu} &= \epsilon \int_{-\infty}^{\infty} w_{uv} \hat{C}_{uv}^* e^{-j\Psi_{uv}} A_{uv} d\boldsymbol{\theta} \\ &+ (1 - \epsilon) PN e^{-j\Psi_u} \delta_{uv} I \\ H &= \begin{bmatrix} H_{00} & H_{01} & \cdots & H_{0,M-1} \\ H_{10} & H_{11} & \cdots & H_{1,M-1} \\ \vdots & \vdots & \ddots & \vdots \\ H_{M-1,0} & H_{M-1,1} & \cdots & H_{M-1,M-1} \end{bmatrix} \end{aligned}$$

The problem has been simplified to a quadratic problem, but the non-convex constraints remain. To deal with the constraint, we use the approach presented in [38], in which the optimization is performed without considering

the constraints and then the solution is projected back to the feasible set of solutions. The minimization and projection steps are:

$$\mathbf{b} \text{ fixed: } \mathbf{a}^* = F^{-1} H^H \mathbf{b} \quad (24)$$

$$\mathbf{a}^* \leftarrow e^{j \arg(\mathbf{a}^*)} \quad (25)$$

$$\mathbf{a} \text{ fixed: } \mathbf{b}^* = G^{-1} H \mathbf{a} \quad (26)$$

$$\mathbf{b}_v^* \leftarrow \mathbf{b}_v^* \sqrt{\frac{PN}{\mathbf{b}_v^{*H} \mathbf{b}_v^*}} \quad (27)$$

The objective function Γ in Equation 22 and Equation 23 presents a minimum in the unconstrained space of \mathbf{a} and \mathbf{b} if, and only if, the Hessian matrix of Γ is positive-definite, which implies that the matrices F and G should be positive-definite. To ensure positive-definiteness of F and G , we additionally apply a diagonal loading given by $F \leftarrow F + \lambda_F I$ and $G \leftarrow G + \lambda_G I$, with λ_F and λ_G greater than the absolute value of the most negative eigenvalue of F and G , respectively. A similar technique is done in [43]. Notice that the positive definiteness of F and G also ensures that the objective function decreases at each of the steps in Equation 24 and Equation 26.

The Auto- and Cross-Ambiguity Functions are synthesized by providing the desired C_{uv} functions and the weight functions w_{uv} , and then iteratively optimizing \mathbf{a} and \mathbf{b} until a convergence criterion is met. This gives flexibility to choose a region of interest in the space of $\boldsymbol{\theta}$ as well as a desired shape for the functions.

7. NUMERICAL EXPERIMENTS

This section presents some numerical experiments to test the proposed CAF synthesis algorithm and evaluate its performance against classical analytically derived codes. In the simulations, we utilized two transmitters and two receiving filters, with each filter linked to a specific transmitter. The AAF was evaluated by processing the waveform of the first transmitter using the first filter, while the CAF was assessed by processing the first transmitter's waveform with the filter associated with the second transmitter. The remaining combinations of transmitted waveforms and filters were not evaluated, as they were deemed redundant for this analysis.

Initially, we tested the algorithm's capability to synthesize arbitrary AAF shapes while maintaining orthogonality in the CAF. In the second experiment, we analyzed the effect of using multiple pulses, each with different codes, on the synthesis algorithm. The goal AAF was set to a thumbtack shape, while the goal CAF was set to zero. The synthesis algorithm was executed multiple times with an increasing number of pulses. In the third experiment, we evaluated the algorithm's performance in synthesizing waveforms with an ideal AAF (thumbtack shape) and zero CAF. Strategies included using a digital impulse function with a guard mask, a Gaussian function,

and a sinc function for the main lobe to enhance synthesis stability and quality.

In the experiments, we evaluated performance using the following metrics: Peak Sidelobe Level Ratio (PSLR) and Averaged Sidelobe Level Ratio (ASLR) [44] for the AAF, along with Peak Sidelobe Level (PSL) and Averaged Sidelobe Level (ASL) for the CAF. These metrics were assessed across specific subsets of the target parameter space referred to as “slices”. The slices include the range-speed plane, range axis, and speed axis. Lower values of these metrics indicate better performance, providing a comprehensive evaluation of the algorithm’s synthesis capability across various conditions. Conceptually, the PSLR and ASLR are defined as

$$\text{PSLR} = 20 \log \left(\frac{\text{Sidelobe Peak}}{\text{Mainlobe peak}} \right) \quad (28)$$

$$\text{ASLR} = 10 \log \left(\frac{\int (\text{Sidelobe})^2}{\int (\text{Sidelobe volume})} \frac{\text{Mainlobe volume}}{\int (\text{Hauptkeule})^2} \right) \quad (29)$$

Table 1 presents the common parameters used in the simulations. Test-specific parameters are described in the text of the corresponding test.

Table 1. Common parameters used in numerical experiments.

Parameter	Value
Pulse width	1 ms
Carrier frequency	1.5 GHz
PRI	0.02 s
Number of pulses	10
Code length (per pulse)	256
Number of transmitters	2

7.1. Chirp-like and Tracking Application

First, the goal AAF is set as a diagonal of 1 values and the other values are 0. The goal CAF is set to zero. From Figure 4, we notice that the generated waveforms are very similar to a chirp waveform, except for the time-stepped phase shifts and an amplitude modulation for the Rx filters. Although the result is not impressive in the sense of obtaining a new waveform code, it is interesting to see that the synthesis algorithm was able to generate the phase code that reproduces the linear frequency modulation of the chip waveform, in order to approximate the goal AAF. In the frequency domain, Figure 5, we notice the resemblance with the chirp frequency spectrum and we see that the generated chirps are placed in different center frequencies. This result comes from the orthogonality requirement enforced by the goal zero CAF.

Second, we consider a tracking application, in which the range and Doppler speed of the target are already known up to some degree of uncertainty, and the detection aims

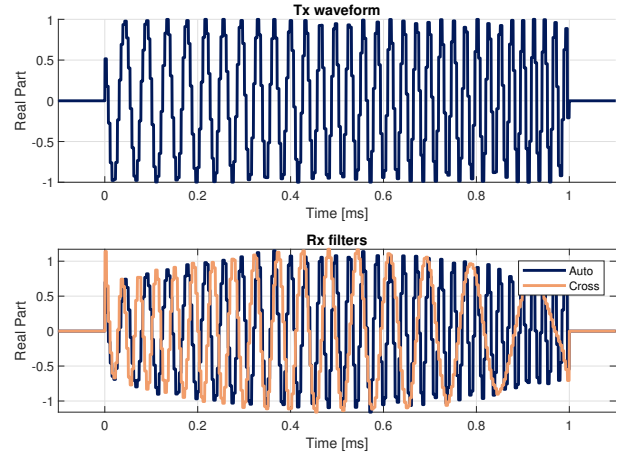


Figure 4. Chirp-like – First pulse in time domain.

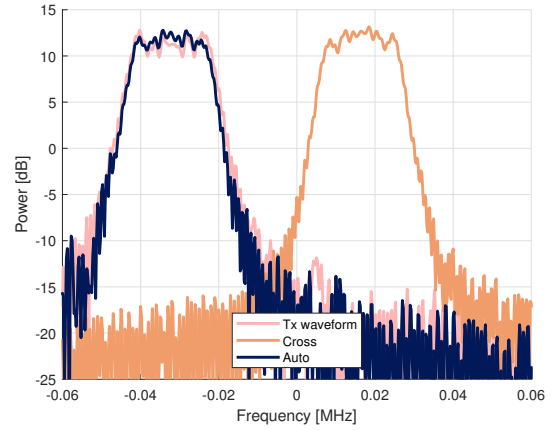


Figure 5. Chirp-like – First pulse in frequency domain.

to correct the predictions. Therefore, it is not necessary to search in the entire target parameter space, and one can focus on a smaller region around the origin instead. In this case, high sidelobes outside the search region are irrelevant and we can ignore the optimization in that region. To test this, we reduce the optimization region to $[0, 50]$ km in range and $[-1.125, 1.125]$ km/s in radial speed. The goal AAF is set to an impulse function (discrete unit sample function) with value 1 at origin and 0 everywhere else. The CAF is set to zero. The weight function is 1 everywhere except in a guard region around the origin. The reason for this guard region is to avoid numeric instabilities as the algorithm would try to optimize a region that is impossible to nullify due to resolution. The resulting AAF and CAF are presented in Figures 6 and 7, where we notice an average sidelobe level as low as -50 dB in the optimization region. The exact numeric values for the calculated metrics are presented in Table 2. With this test, we demonstrate the effectiveness of the proposed algorithm in optimizing waveforms specifically tailored for tracking applications.

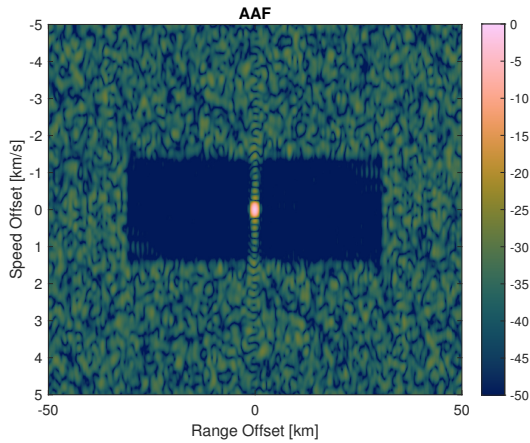


Figure 6. Tracking application – AAF.

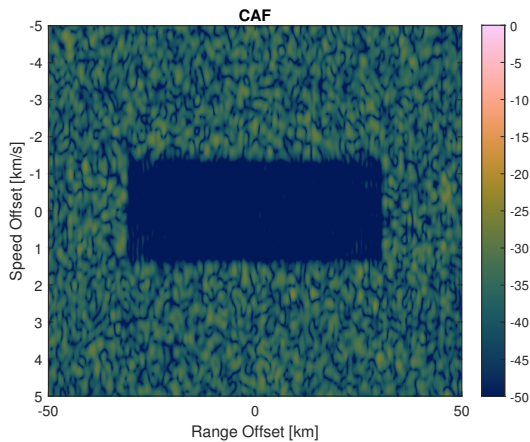


Figure 7. Tracking application – CAF.

Table 2. Performance metrics for tracking application (dB).

	Metric	RVA-Slice	RV-Slice	R-Slice	V-Slice
AAF	Loss	0,26			
	PSLR	-5,85	-20,91	-51,46	-20,91
	ASLR	-11,41	-30,24	-52,69	-23,95
CAF	PSL	-24,45	-44,68	-58,93	-56,27
	ASL	-36,64	-60,18	-65,46	-62,47

7.2. Effect of multiple pulses

This experiment is aimed to investigate the impact of utilizing multiple pulses, each encoded with distinct codes, on the synthesis of Ambiguity Functions. The objective was to assess whether increasing the number of pulses could effectively improve the sidelobe level reduction and decrease cross-correlation interference.

To proceed with this analysis, we established the target AAF as a thumbtack shape with a guard region around the mainlobe. The goal CAF was set to zero to ensure orthogonality. The optimization region was defined as

$[0, 300]$ km in range and $[-10, 10]$ km/s in radial speed. The synthesis algorithm was executed successively, with the number of pulses incrementally increasing in each run, from 1 pulse up until 10 pulses. The AAF and CAF metrics were then evaluated for each generated code set and are compared across the different configurations for the number of pulses.

Figure 8 presents the optimization objective function versus iteration for the different configurations of number of pulses. The absolute values of this objective function do not tell us much, except that the smaller the value the better the synthesized AF approximate the goal AF. However, the values are comparable to each other because we normalized this metric in terms of the number of pulses. From this figure, we notice that all the configurations converge and, indeed, increasing the number of pulses improves the final value of the objective function.

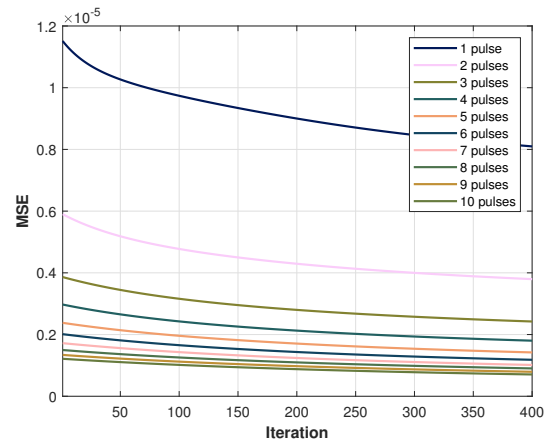


Figure 8. Objective function versus iteration.

Figures 9 and 10 illustrate how the metrics for the AAF and CAF, respectively, change as the number of pulses increases. From the figures, we notice a slight decrease in the AAF metrics followed by a stagnation, while in the CAF metrics we notice a monotonous decrease.

7.3. Thumbtack

In the last numerical experiment, we assessed the performance of the synthesis algorithm in generating waveforms that closely match ideal Auto Ambiguity Functions (AAFs) and Cross Ambiguity Functions (CAFs).

Initially, we set the goal AAF as a digital impulse function with a guard region. In the second and third optimizations, we applied a Gaussian shape and a Sinc shape, respectively, for the peak of the AAF. The Gaussian full width at half maximum and the sinc width were set to be equal to the size of the resolutions. By applying a guard region in the first optimization, we exclude those points during the synthesis process, which typically reduces the number of points contributing to the main lobe

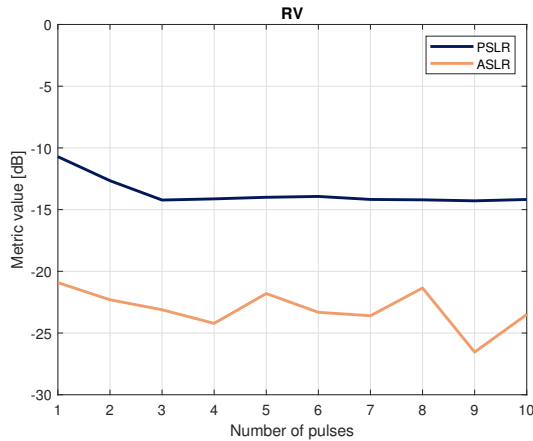


Figure 9. AAF metrics versus number of pulses – RV-cut.

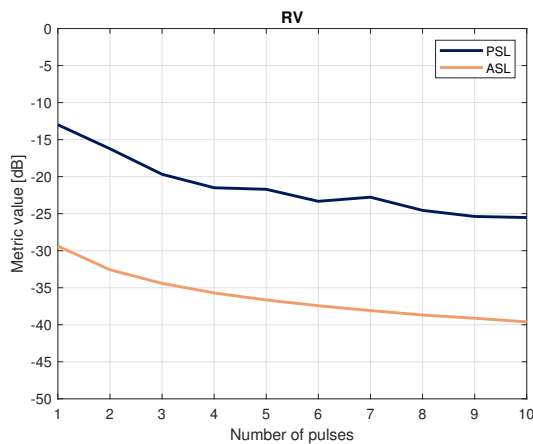


Figure 10. CAF metrics versus number of pulses – RV-cut.

and, consequently, diminishes its overall significance relative to the sidelobes. By setting the goal AAF to a Gaussian/Sinc shape, we effectively circumvented this issue of discarding points, ensuring a more balanced representation of the main lobe. Moreover, we set the values outside the mainlobe to -30 dB instead of 0. The reasoning is that by pushing the energy to zero in some points, one could end up with high sidelobes in points where the AF is not optimized, due to the constant volume property of the AF. Meanwhile, aiming for a more relaxed objective function could try to obtain a more uniform and balanced sidelobe level, with smaller peaks. The goal AAF for the Gaussian shaped AAF is presented in Figure 11, for the Sinc-shaped AAF, it is presented in Figure 12. The goal CAF is set to -30 dB for both optimizations.

To test the FHSS technique in an asynchronous CDMA, one must choose a code that shifts the frequency of the waveform in such a way that conflicts are minimized when the signal is correlated with a time-delayed and frequency-shifted copy of itself. This is none other than the Costas waveform. In other words, the Costas waveform can be seen as a special case of FHSS when applied

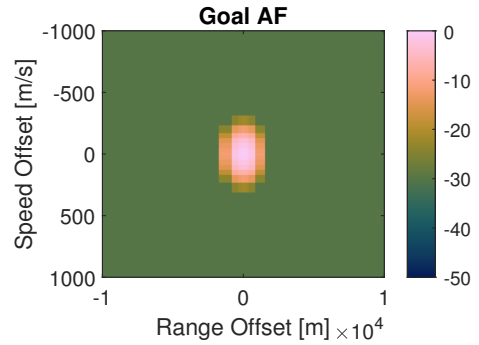


Figure 11. Gaussian-shaped goal AAF.

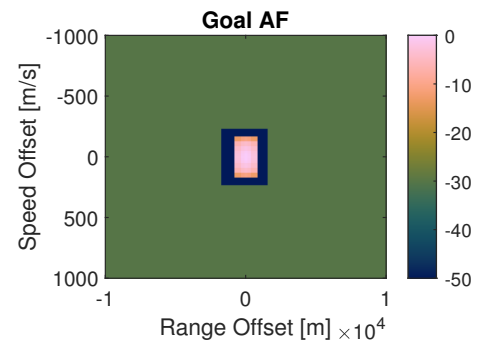


Figure 12. Sinc-shaped goal AAF.

to the rectangular pulse. We employ a hybrid approach, in which multiple Costas codes are used together with DSSS (similar to [45]). We assign a different Costas code to each transmitter. A different optimization run was made for the case where no FHSS is applied and for the case where the Costas code is used for FHSS.

We compared the obtained optimized codes with classical analytically derived codes: Walsh-Hadamard, M-Sequence, Gold, and Kasami. Each of these code sets has several codes that can be used to distinguish between transmitters. We arbitrarily chose a pair of codes from each set and assigned one code to each transmitter. Moreover, we combined a DSSS using the mentioned analytically generated codes with the FHSS using the Costas code. In addition to the classical codes, we implemented the optimization methods from [35] and [36]. However, because their methods consider only the single pulse case, we applied some modifications to the methods, in the direction of considering a train of pulses as a single waveform and then applying the single pulse methods of the references.

The resulting waveforms had their performance evaluated in terms of the defined metrics and the results are listed in Table 3, for AAF metrics, and in Table 4, for CAF metrics. The SNR loss is presented in Table 5. These tables indicate that the optimized waveforms, either with the proposed CAF synthesis approach or with the methods from Chen et al [35] and He et al. [36], present better orthogonality properties (lowest CAF metrics) than the

Table 3. Results of the performance metrics for AAF.

	RV	R	V																																																																																																									
PSLR	<table border="1"> <thead> <tr> <th rowspan="2">DSSS</th> <th colspan="2">FHSS</th> </tr> <tr> <th>None</th> <th>Costas</th> </tr> </thead> <tbody> <tr><td>None</td><td>-</td><td>-14,18</td></tr> <tr><td>Walsh-Hadamard</td><td>-3,13</td><td>-14,25</td></tr> <tr><td>M-Sequence</td><td>-13,79</td><td>-14,17</td></tr> <tr><td>Gold</td><td>-14,22</td><td>-14,63</td></tr> <tr><td>Kasami</td><td>-13,95</td><td>-14,46</td></tr> <tr><td>Chen et al.</td><td>-12,96</td><td>-13,02</td></tr> <tr><td>He et al.</td><td>-14,11</td><td>-14,23</td></tr> <tr><td>Optim. (Impulse)</td><td>-14,13</td><td>-14,25</td></tr> <tr><td>Optim. (Gaussian)</td><td>-14,23</td><td>-14,24</td></tr> <tr><td>Optim. (Sinc)</td><td>-14,22</td><td>-14,09</td></tr> </tbody> </table> <p>(a) AAF - PSLR in RV map</p>	DSSS	FHSS		None	Costas	None	-	-14,18	Walsh-Hadamard	-3,13	-14,25	M-Sequence	-13,79	-14,17	Gold	-14,22	-14,63	Kasami	-13,95	-14,46	Chen et al.	-12,96	-13,02	He et al.	-14,11	-14,23	Optim. (Impulse)	-14,13	-14,25	Optim. (Gaussian)	-14,23	-14,24	Optim. (Sinc)	-14,22	-14,09	<table border="1"> <thead> <tr> <th rowspan="2">DSSS</th> <th colspan="2">FHSS</th> </tr> <tr> <th>None</th> <th>Costas</th> </tr> </thead> <tbody> <tr><td>None</td><td>-</td><td>-19,33</td></tr> <tr><td>Walsh-Hadamard</td><td>-3,13</td><td>-20,89</td></tr> <tr><td>M-Sequence</td><td>-23,59</td><td>-21,11</td></tr> <tr><td>Gold</td><td>-18,29</td><td>-22,43</td></tr> <tr><td>Kasami</td><td>-18,55</td><td>-23,26</td></tr> <tr><td>Chen et al.</td><td>-22,62</td><td>-22,45</td></tr> <tr><td>He et al.</td><td>-27,84</td><td>-27,64</td></tr> <tr><td>Optim. (Impulse)</td><td>-19,58</td><td>-30,92</td></tr> <tr><td>Optim. (Gaussian)</td><td>-19,03</td><td>-29,67</td></tr> <tr><td>Optim. (Sinc)</td><td>-20,86</td><td>-28,85</td></tr> </tbody> </table> <p>(b) AAF - PSLR in R map</p>	DSSS	FHSS		None	Costas	None	-	-19,33	Walsh-Hadamard	-3,13	-20,89	M-Sequence	-23,59	-21,11	Gold	-18,29	-22,43	Kasami	-18,55	-23,26	Chen et al.	-22,62	-22,45	He et al.	-27,84	-27,64	Optim. (Impulse)	-19,58	-30,92	Optim. (Gaussian)	-19,03	-29,67	Optim. (Sinc)	-20,86	-28,85	<table border="1"> <thead> <tr> <th rowspan="2">DSSS</th> <th colspan="2">FHSS</th> </tr> <tr> <th>None</th> <th>Costas</th> </tr> </thead> <tbody> <tr><td>None</td><td>-</td><td>-14,18</td></tr> <tr><td>Walsh-Hadamard</td><td>-14,80</td><td>-14,25</td></tr> <tr><td>M-Sequence</td><td>-13,79</td><td>-14,38</td></tr> <tr><td>Gold</td><td>-14,22</td><td>-14,75</td></tr> <tr><td>Kasami</td><td>-13,95</td><td>-14,46</td></tr> <tr><td>Chen et al.</td><td>-12,96</td><td>-13,02</td></tr> <tr><td>He et al.</td><td>-14,11</td><td>-14,23</td></tr> <tr><td>Optim. (Impulse)</td><td>-14,13</td><td>-14,25</td></tr> <tr><td>Optim. (Gaussian)</td><td>-14,23</td><td>-14,24</td></tr> <tr><td>Optim. (Sinc)</td><td>-14,22</td><td>-14,09</td></tr> </tbody> </table> <p>(c) AAF - PSLR in V map</p>	DSSS	FHSS		None	Costas	None	-	-14,18	Walsh-Hadamard	-14,80	-14,25	M-Sequence	-13,79	-14,38	Gold	-14,22	-14,75	Kasami	-13,95	-14,46	Chen et al.	-12,96	-13,02	He et al.	-14,11	-14,23	Optim. (Impulse)	-14,13	-14,25	Optim. (Gaussian)	-14,23	-14,24	Optim. (Sinc)	-14,22	-14,09
	DSSS		FHSS																																																																																																									
		None	Costas																																																																																																									
	None	-	-14,18																																																																																																									
	Walsh-Hadamard	-3,13	-14,25																																																																																																									
	M-Sequence	-13,79	-14,17																																																																																																									
	Gold	-14,22	-14,63																																																																																																									
	Kasami	-13,95	-14,46																																																																																																									
	Chen et al.	-12,96	-13,02																																																																																																									
	He et al.	-14,11	-14,23																																																																																																									
Optim. (Impulse)	-14,13	-14,25																																																																																																										
Optim. (Gaussian)	-14,23	-14,24																																																																																																										
Optim. (Sinc)	-14,22	-14,09																																																																																																										
DSSS	FHSS																																																																																																											
	None	Costas																																																																																																										
None	-	-19,33																																																																																																										
Walsh-Hadamard	-3,13	-20,89																																																																																																										
M-Sequence	-23,59	-21,11																																																																																																										
Gold	-18,29	-22,43																																																																																																										
Kasami	-18,55	-23,26																																																																																																										
Chen et al.	-22,62	-22,45																																																																																																										
He et al.	-27,84	-27,64																																																																																																										
Optim. (Impulse)	-19,58	-30,92																																																																																																										
Optim. (Gaussian)	-19,03	-29,67																																																																																																										
Optim. (Sinc)	-20,86	-28,85																																																																																																										
DSSS	FHSS																																																																																																											
	None	Costas																																																																																																										
None	-	-14,18																																																																																																										
Walsh-Hadamard	-14,80	-14,25																																																																																																										
M-Sequence	-13,79	-14,38																																																																																																										
Gold	-14,22	-14,75																																																																																																										
Kasami	-13,95	-14,46																																																																																																										
Chen et al.	-12,96	-13,02																																																																																																										
He et al.	-14,11	-14,23																																																																																																										
Optim. (Impulse)	-14,13	-14,25																																																																																																										
Optim. (Gaussian)	-14,23	-14,24																																																																																																										
Optim. (Sinc)	-14,22	-14,09																																																																																																										
ASLR	<table border="1"> <thead> <tr> <th rowspan="2">DSSS</th> <th colspan="2">FHSS</th> </tr> <tr> <th>None</th> <th>Costas</th> </tr> </thead> <tbody> <tr><td>None</td><td>-</td><td>-19,34</td></tr> <tr><td>Walsh-Hadamard</td><td>-20,71</td><td>-15,54</td></tr> <tr><td>M-Sequence</td><td>-18,41</td><td>-19,38</td></tr> <tr><td>Gold</td><td>-15,11</td><td>-17,78</td></tr> <tr><td>Kasami</td><td>-16,35</td><td>-18,38</td></tr> <tr><td>Chen et al.</td><td>-17,55</td><td>-16,72</td></tr> <tr><td>He et al.</td><td>-24,91</td><td>-24,98</td></tr> <tr><td>Optim. (Impulse)</td><td>-23,56</td><td>-23,97</td></tr> <tr><td>Optim. (Gaussian)</td><td>-24,34</td><td>-23,90</td></tr> <tr><td>Optim. (Sinc)</td><td>-24,88</td><td>-24,62</td></tr> </tbody> </table> <p>(d) AAF - ASLR in RV map</p>	DSSS	FHSS		None	Costas	None	-	-19,34	Walsh-Hadamard	-20,71	-15,54	M-Sequence	-18,41	-19,38	Gold	-15,11	-17,78	Kasami	-16,35	-18,38	Chen et al.	-17,55	-16,72	He et al.	-24,91	-24,98	Optim. (Impulse)	-23,56	-23,97	Optim. (Gaussian)	-24,34	-23,90	Optim. (Sinc)	-24,88	-24,62	<table border="1"> <thead> <tr> <th rowspan="2">DSSS</th> <th colspan="2">FHSS</th> </tr> <tr> <th>None</th> <th>Costas</th> </tr> </thead> <tbody> <tr><td>None</td><td>-</td><td>-24,92</td></tr> <tr><td>Walsh-Hadamard</td><td>-15,29</td><td>-20,84</td></tr> <tr><td>M-Sequence</td><td>-24,39</td><td>-22,84</td></tr> <tr><td>Gold</td><td>-21,35</td><td>-22,78</td></tr> <tr><td>Kasami</td><td>-21,51</td><td>-23,42</td></tr> <tr><td>Chen et al.</td><td>-25,27</td><td>-22,83</td></tr> <tr><td>He et al.</td><td>-29,35</td><td>-31,21</td></tr> <tr><td>Optim. (Impulse)</td><td>-31,43</td><td>-33,59</td></tr> <tr><td>Optim. (Gaussian)</td><td>-30,21</td><td>-30,17</td></tr> <tr><td>Optim. (Sinc)</td><td>-31,75</td><td>-31,67</td></tr> </tbody> </table> <p>(e) AAF - ASLR in R map</p>	DSSS	FHSS		None	Costas	None	-	-24,92	Walsh-Hadamard	-15,29	-20,84	M-Sequence	-24,39	-22,84	Gold	-21,35	-22,78	Kasami	-21,51	-23,42	Chen et al.	-25,27	-22,83	He et al.	-29,35	-31,21	Optim. (Impulse)	-31,43	-33,59	Optim. (Gaussian)	-30,21	-30,17	Optim. (Sinc)	-31,75	-31,67	<table border="1"> <thead> <tr> <th rowspan="2">DSSS</th> <th colspan="2">FHSS</th> </tr> <tr> <th>None</th> <th>Costas</th> </tr> </thead> <tbody> <tr><td>None</td><td>-</td><td>-23,01</td></tr> <tr><td>Walsh-Hadamard</td><td>-25,93</td><td>-23,41</td></tr> <tr><td>M-Sequence</td><td>-23,47</td><td>-24,34</td></tr> <tr><td>Gold</td><td>-23,99</td><td>-24,06</td></tr> <tr><td>Kasami</td><td>-24,01</td><td>-23,58</td></tr> <tr><td>Chen et al.</td><td>-22,94</td><td>-22,17</td></tr> <tr><td>He et al.</td><td>-25,78</td><td>-25,13</td></tr> <tr><td>Optim. (Impulse)</td><td>-26,00</td><td>-25,27</td></tr> <tr><td>Optim. (Gaussian)</td><td>-25,91</td><td>-25,31</td></tr> <tr><td>Optim. (Sinc)</td><td>-25,63</td><td>-24,85</td></tr> </tbody> </table> <p>(f) AAF - ASLR in V map</p>	DSSS	FHSS		None	Costas	None	-	-23,01	Walsh-Hadamard	-25,93	-23,41	M-Sequence	-23,47	-24,34	Gold	-23,99	-24,06	Kasami	-24,01	-23,58	Chen et al.	-22,94	-22,17	He et al.	-25,78	-25,13	Optim. (Impulse)	-26,00	-25,27	Optim. (Gaussian)	-25,91	-25,31	Optim. (Sinc)	-25,63	-24,85
	DSSS		FHSS																																																																																																									
		None	Costas																																																																																																									
	None	-	-19,34																																																																																																									
	Walsh-Hadamard	-20,71	-15,54																																																																																																									
	M-Sequence	-18,41	-19,38																																																																																																									
	Gold	-15,11	-17,78																																																																																																									
	Kasami	-16,35	-18,38																																																																																																									
	Chen et al.	-17,55	-16,72																																																																																																									
	He et al.	-24,91	-24,98																																																																																																									
Optim. (Impulse)	-23,56	-23,97																																																																																																										
Optim. (Gaussian)	-24,34	-23,90																																																																																																										
Optim. (Sinc)	-24,88	-24,62																																																																																																										
DSSS	FHSS																																																																																																											
	None	Costas																																																																																																										
None	-	-24,92																																																																																																										
Walsh-Hadamard	-15,29	-20,84																																																																																																										
M-Sequence	-24,39	-22,84																																																																																																										
Gold	-21,35	-22,78																																																																																																										
Kasami	-21,51	-23,42																																																																																																										
Chen et al.	-25,27	-22,83																																																																																																										
He et al.	-29,35	-31,21																																																																																																										
Optim. (Impulse)	-31,43	-33,59																																																																																																										
Optim. (Gaussian)	-30,21	-30,17																																																																																																										
Optim. (Sinc)	-31,75	-31,67																																																																																																										
DSSS	FHSS																																																																																																											
	None	Costas																																																																																																										
None	-	-23,01																																																																																																										
Walsh-Hadamard	-25,93	-23,41																																																																																																										
M-Sequence	-23,47	-24,34																																																																																																										
Gold	-23,99	-24,06																																																																																																										
Kasami	-24,01	-23,58																																																																																																										
Chen et al.	-22,94	-22,17																																																																																																										
He et al.	-25,78	-25,13																																																																																																										
Optim. (Impulse)	-26,00	-25,27																																																																																																										
Optim. (Gaussian)	-25,91	-25,31																																																																																																										
Optim. (Sinc)	-25,63	-24,85																																																																																																										

Table 4. Results of the performance metrics for CAF.

	RV	R	V																																																																																																									
PSL	<table border="1"> <thead> <tr> <th rowspan="2">DSSS</th> <th colspan="2">FHSS</th> </tr> <tr> <th>None</th> <th>Costas</th> </tr> </thead> <tbody> <tr><td>None</td><td>-</td><td>-17,19</td></tr> <tr><td>Walsh-Hadamard</td><td>-18,40</td><td>-17,66</td></tr> <tr><td>M-Sequence</td><td>-16,12</td><td>-18,55</td></tr> <tr><td>Gold</td><td>-16,93</td><td>-18,86</td></tr> <tr><td>Kasami</td><td>-12,61</td><td>-18,09</td></tr> <tr><td>Chen et al.</td><td>-25,92</td><td>-26,84</td></tr> <tr><td>He et al.</td><td>-24,85</td><td>-26,45</td></tr> <tr><td>Optim. (Impulse)</td><td>-25,45</td><td>-26,89</td></tr> <tr><td>Optim. (Gaussian)</td><td>-24,92</td><td>-26,42</td></tr> <tr><td>Optim. (Sinc)</td><td>-26,02</td><td>-26,96</td></tr> </tbody> </table> <p>(a) CAF - PSL in RV map</p>	DSSS	FHSS		None	Costas	None	-	-17,19	Walsh-Hadamard	-18,40	-17,66	M-Sequence	-16,12	-18,55	Gold	-16,93	-18,86	Kasami	-12,61	-18,09	Chen et al.	-25,92	-26,84	He et al.	-24,85	-26,45	Optim. (Impulse)	-25,45	-26,89	Optim. (Gaussian)	-24,92	-26,42	Optim. (Sinc)	-26,02	-26,96	<table border="1"> <thead> <tr> <th rowspan="2">DSSS</th> <th colspan="2">FHSS</th> </tr> <tr> <th>None</th> <th>Costas</th> </tr> </thead> <tbody> <tr><td>None</td><td>-</td><td>-19,85</td></tr> <tr><td>Walsh-Hadamard</td><td>-28,02</td><td>-20,98</td></tr> <tr><td>M-Sequence</td><td>-18,28</td><td>-19,48</td></tr> <tr><td>Gold</td><td>-18,42</td><td>-21,89</td></tr> <tr><td>Kasami</td><td>-17,89</td><td>-21,94</td></tr> <tr><td>Chen et al.</td><td>-30,00</td><td>-29,34</td></tr> <tr><td>He et al.</td><td>-28,90</td><td>-28,77</td></tr> <tr><td>Optim. (Impulse)</td><td>-26,77</td><td>-29,80</td></tr> <tr><td>Optim. (Gaussian)</td><td>-28,74</td><td>-29,56</td></tr> <tr><td>Optim. (Sinc)</td><td>-26,81</td><td>-29,40</td></tr> </tbody> </table> <p>(b) CAF - PSL in R map</p>	DSSS	FHSS		None	Costas	None	-	-19,85	Walsh-Hadamard	-28,02	-20,98	M-Sequence	-18,28	-19,48	Gold	-18,42	-21,89	Kasami	-17,89	-21,94	Chen et al.	-30,00	-29,34	He et al.	-28,90	-28,77	Optim. (Impulse)	-26,77	-29,80	Optim. (Gaussian)	-28,74	-29,56	Optim. (Sinc)	-26,81	-29,40	<table border="1"> <thead> <tr> <th rowspan="2">DSSS</th> <th colspan="2">FHSS</th> </tr> <tr> <th>None</th> <th>Costas</th> </tr> </thead> <tbody> <tr><td>None</td><td>-</td><td>-20,21</td></tr> <tr><td>Walsh-Hadamard</td><td>-20,53</td><td>-19,64</td></tr> <tr><td>M-Sequence</td><td>-18,48</td><td>-20,62</td></tr> <tr><td>Gold</td><td>-20,53</td><td>-20,86</td></tr> <tr><td>Kasami</td><td>-13,61</td><td>-21,45</td></tr> <tr><td>Chen et al.</td><td>-28,81</td><td>-27,26</td></tr> <tr><td>He et al.</td><td>-28,27</td><td>-28,06</td></tr> <tr><td>Optim. (Impulse)</td><td>-26,33</td><td>-28,68</td></tr> <tr><td>Optim. (Gaussian)</td><td>-27,79</td><td>-29,48</td></tr> <tr><td>Optim. (Sinc)</td><td>-26,81</td><td>-29,16</td></tr> </tbody> </table> <p>(c) CAF - PSL in V map</p>	DSSS	FHSS		None	Costas	None	-	-20,21	Walsh-Hadamard	-20,53	-19,64	M-Sequence	-18,48	-20,62	Gold	-20,53	-20,86	Kasami	-13,61	-21,45	Chen et al.	-28,81	-27,26	He et al.	-28,27	-28,06	Optim. (Impulse)	-26,33	-28,68	Optim. (Gaussian)	-27,79	-29,48	Optim. (Sinc)	-26,81	-29,16
	DSSS		FHSS																																																																																																									
		None	Costas																																																																																																									
	None	-	-17,19																																																																																																									
	Walsh-Hadamard	-18,40	-17,66																																																																																																									
	M-Sequence	-16,12	-18,55																																																																																																									
	Gold	-16,93	-18,86																																																																																																									
	Kasami	-12,61	-18,09																																																																																																									
	Chen et al.	-25,92	-26,84																																																																																																									
	He et al.	-24,85	-26,45																																																																																																									
Optim. (Impulse)	-25,45	-26,89																																																																																																										
Optim. (Gaussian)	-24,92	-26,42																																																																																																										
Optim. (Sinc)	-26,02	-26,96																																																																																																										
DSSS	FHSS																																																																																																											
	None	Costas																																																																																																										
None	-	-19,85																																																																																																										
Walsh-Hadamard	-28,02	-20,98																																																																																																										
M-Sequence	-18,28	-19,48																																																																																																										
Gold	-18,42	-21,89																																																																																																										
Kasami	-17,89	-21,94																																																																																																										
Chen et al.	-30,00	-29,34																																																																																																										
He et al.	-28,90	-28,77																																																																																																										
Optim. (Impulse)	-26,77	-29,80																																																																																																										
Optim. (Gaussian)	-28,74	-29,56																																																																																																										
Optim. (Sinc)	-26,81	-29,40																																																																																																										
DSSS	FHSS																																																																																																											
	None	Costas																																																																																																										
None	-	-20,21																																																																																																										
Walsh-Hadamard	-20,53	-19,64																																																																																																										
M-Sequence	-18,48	-20,62																																																																																																										
Gold	-20,53	-20,86																																																																																																										
Kasami	-13,61	-21,45																																																																																																										
Chen et al.	-28,81	-27,26																																																																																																										
He et al.	-28,27	-28,06																																																																																																										
Optim. (Impulse)	-26,33	-28,68																																																																																																										
Optim. (Gaussian)	-27,79	-29,48																																																																																																										
Optim. (Sinc)	-26,81	-29,16																																																																																																										
ASL	<table border="1"> <thead> <tr> <th rowspan="2">DSSS</th> <th colspan="2">FHSS</th> </tr> <tr> <th>None</th> <th>Costas</th> </tr> </thead> <tbody> <tr><td>None</td><td>-</td><td>-31,50</td></tr> <tr><td>Walsh-Hadamard</td><td>-34,40</td><td>-31,04</td></tr> <tr><td>M-Sequence</td><td>-29,69</td><td>-33,34</td></tr> <tr><td>Gold</td><td>-29,61</td><td>-33,09</td></tr> <tr><td>Kasami</td><td>-29,38</td><td>-33,08</td></tr> <tr><td>Chen et al.</td><td>-39,72</td><td>-40,39</td></tr> <tr><td>He et al.</td><td>-38,99</td><td>-40,32</td></tr> <tr><td>Optim. (Impulse)</td><td>-39,59</td><td>-40,28</td></tr> <tr><td>Optim. (Gaussian)</td><td>-39,54</td><td>-40,23</td></tr> <tr><td>Optim. (Sinc)</td><td>-39,50</td><td>-40,30</td></tr> </tbody> </table> <p>(d) CAF - ASL in RV map</p>	DSSS	FHSS		None	Costas	None	-	-31,50	Walsh-Hadamard	-34,40	-31,04	M-Sequence	-29,69	-33,34	Gold	-29,61	-33,09	Kasami	-29,38	-33,08	Chen et al.	-39,72	-40,39	He et al.	-38,99	-40,32	Optim. (Impulse)	-39,59	-40,28	Optim. (Gaussian)	-39,54	-40,23	Optim. (Sinc)	-39,50	-40,30	<table border="1"> <thead> <tr> <th rowspan="2">DSSS</th> <th colspan="2">FHSS</th> </tr> <tr> <th>None</th> <th>Costas</th> </tr> </thead> <tbody> <tr><td>None</td><td>-</td><td>-30,34</td></tr> <tr><td>Walsh-Hadamard</td><td>-40,19</td><td>-30,25</td></tr> <tr><td>M-Sequence</td><td>-27,79</td><td>-31,91</td></tr> <tr><td>Gold</td><td>-28,92</td><td>-31,75</td></tr> <tr><td>Kasami</td><td>-28,99</td><td>-31,67</td></tr> <tr><td>Chen et al.</td><td>-40,49</td><td>-40,48</td></tr> <tr><td>He et al.</td><td>-39,04</td><td>-40,36</td></tr> <tr><td>Optim. (Impulse)</td><td>-39,54</td><td>-40,45</td></tr> <tr><td>Optim. (Gaussian)</td><td>-39,53</td><td>-40,21</td></tr> <tr><td>Optim. (Sinc)</td><td>-39,46</td><td>-40,28</td></tr> </tbody> </table> <p>(e) CAF - ASL in R map</p>	DSSS	FHSS		None	Costas	None	-	-30,34	Walsh-Hadamard	-40,19	-30,25	M-Sequence	-27,79	-31,91	Gold	-28,92	-31,75	Kasami	-28,99	-31,67	Chen et al.	-40,49	-40,48	He et al.	-39,04	-40,36	Optim. (Impulse)	-39,54	-40,45	Optim. (Gaussian)	-39,53	-40,21	Optim. (Sinc)	-39,46	-40,28	<table border="1"> <thead> <tr> <th rowspan="2">DSSS</th> <th colspan="2">FHSS</th> </tr> <tr> <th>None</th> <th>Costas</th> </tr> </thead> <tbody> <tr><td>None</td><td>-</td><td>-29,86</td></tr> <tr><td>Walsh-Hadamard</td><td>-31,71</td><td>-27,91</td></tr> <tr><td>M-Sequence</td><td>-27,37</td><td>-30,12</td></tr> <tr><td>Gold</td><td>-26,55</td><td>-29,55</td></tr> <tr><td>Kasami</td><td>-27,16</td><td>-29,46</td></tr> <tr><td>Chen et al.</td><td>-36,28</td><td>-36,60</td></tr> <tr><td>He et al.</td><td>-35,33</td><td>-36,83</td></tr> <tr><td>Optim. (Impulse)</td><td>-35,65</td><td>-36,79</td></tr> <tr><td>Optim. (Gaussian)</td><td>-35,08</td><td>-37,06</td></tr> <tr><td>Optim. (Sinc)</td><td>-35,44</td><td>-37,15</td></tr> </tbody> </table> <p>(f) CAF - ASL in V map</p>	DSSS	FHSS		None	Costas	None	-	-29,86	Walsh-Hadamard	-31,71	-27,91	M-Sequence	-27,37	-30,12	Gold	-26,55	-29,55	Kasami	-27,16	-29,46	Chen et al.	-36,28	-36,60	He et al.	-35,33	-36,83	Optim. (Impulse)	-35,65	-36,79	Optim. (Gaussian)	-35,08	-37,06	Optim. (Sinc)	-35,44	-37,15
	DSSS		FHSS																																																																																																									
		None	Costas																																																																																																									
	None	-	-31,50																																																																																																									
	Walsh-Hadamard	-34,40	-31,04																																																																																																									
	M-Sequence	-29,69	-33,34																																																																																																									
	Gold	-29,61	-33,09																																																																																																									
	Kasami	-29,38	-33,08																																																																																																									
	Chen et al.	-39,72	-40,39																																																																																																									
	He et al.	-38,99	-40,32																																																																																																									
Optim. (Impulse)	-39,59	-40,28																																																																																																										
Optim. (Gaussian)	-39,54	-40,23																																																																																																										
Optim. (Sinc)	-39,50	-40,30																																																																																																										
DSSS	FHSS																																																																																																											
	None	Costas																																																																																																										
None	-	-30,34																																																																																																										
Walsh-Hadamard	-40,19	-30,25																																																																																																										
M-Sequence	-27,79	-31,91																																																																																																										
Gold	-28,92	-31,75																																																																																																										
Kasami	-28,99	-31,67																																																																																																										
Chen et al.	-40,49	-40,48																																																																																																										
He et al.	-39,04	-40,36																																																																																																										
Optim. (Impulse)	-39,54	-40,45																																																																																																										
Optim. (Gaussian)	-39,53	-40,21																																																																																																										
Optim. (Sinc)	-39,46	-40,28																																																																																																										
DSSS	FHSS																																																																																																											
	None	Costas																																																																																																										
None	-	-29,86																																																																																																										
Walsh-Hadamard	-31,71	-27,91																																																																																																										
M-Sequence	-27,37	-30,12																																																																																																										
Gold	-26,55	-29,55																																																																																																										
Kasami	-27,16	-29,46																																																																																																										
Chen et al.	-36,28	-36,60																																																																																																										
He et al.	-35,33	-36,83																																																																																																										
Optim. (Impulse)	-35,65	-36,79																																																																																																										
Optim. (Gaussian)	-35,08	-37,06																																																																																																										
Optim. (Sinc)	-35,44	-37,15																																																																																																										

Table 5. SNR Loss.

DSSS	FHSS	
	None	Costas
None	-	0,00
Walsh-Hadamard	0,00	0,00
M-Sequence	0,00	0,00
Gold	0,00	0,00
Kasami	0,00	0,00
Chen et al.	6,61	6,61
He et al.	0,00	0,00
Optim. (Impulse)	0,00	0,00
Optim. (Gaussian)	0,00	0,00
Optim. (Sinc)	0,00	0,00

SNR Loss (dB)

classical waveforms. When it comes to sidelobes in the AAF, we notice a worse performance for the Chen et al. waveform while the synthesis approach and the He et al. method still provide good performance. With respect to the SNR loss, all waveforms present zero loss, except for Chen et al.. The reason for this was not fully investigated, but a mistake in our implementation of the method from Chen et al. is not to be discarded.

8. CONCLUSION

In conclusion, the waveforms examined in this study demonstrated satisfactory performance regarding sidelobe levels in both the Auto Ambiguity Function (AAF) and Cross Ambiguity Function (CAF), highlighting that CDMA techniques can effectively facilitate the development of orthogonal waveforms for radar networks. The combination of Direct Sequence Spread Spectrum (DSSS) and Frequency Hopping Spread Spectrum (FHSS) emerges as a robust strategy for generating orthogonal waveforms. Moreover, the use of multiple pulses can enhance sidelobe cancellation; however, it necessitates careful phase compensation to address challenges posed by high speeds and accelerations. Additionally, the AF synthesis method provides a straightforward, flexible approach with deterministic convergence, allowing for efficient waveform design.

ACKNOWLEDGMENTS

The project on which this report is based was funded by the German Federal Ministry for Economic Affairs and Climate Action under the funding code 50 LZ 2005. Responsibility for the content of this publication lies with the author.

The authors acknowledge the use of AI technology (Fh-Genie) for proofreading and enhancing the readability of the manuscript.

REFERENCES

1. B. Sklar, *Digital Communications: Fundamentals and Applications*. Prentice Hall PTR, 2nd ed., 2001.
2. H. Sun, F. Brigrui, and M. Lesturgie, "Analysis and comparison of MIMO radar waveforms," in *Radar Conference (Radar), 2014 International*, pp. 1–6, IEEE, 2014.
3. J. Seberry, B. J. Wysocki, and T. A. Wysocki, "Golay sequences for DS CDMA applications," in *Sixth International Symposium on DSP for Communications Systems (DSPCS'02)*, pp. 103–108, TITR, Wollongong, 2002.
4. M. Dávideková, M. Greguš ml., P. Farkaš, and M. Rákus, "Applications of complete complementary codes and propositions for future research areas of these codes," *Procedia Computer Science*, vol. 83, pp. 592–599, 2016.
5. L. Tian, Y. Li, and C. Xu, "Multiple complete complementary codes with inter-set zero cross-correlation zone," *IEEE Transactions on Communications*, vol. 68, no. 3, pp. 1925–1936, 2020.
6. B. Moran, "Mathematics of radar," in *Twentieth Century Harmonic Analysis — A Celebration* (J. S. Byrnes, ed.), pp. 295–328, Springer Netherlands, 2001.
7. J. Zhang, C. Shi, X. Qiu, and Y. Wu, "Shaping radar ambiguity function by 1-phase unimodular sequence," *IEEE Sensors Journal*, vol. 16, no. 14, pp. 5648–5659, 2016.
8. F. Wang, S. Feng, J. Yin, C. Pang, Y. Li, and X. Wang, "Unimodular sequence and receiving filter design for local ambiguity function shaping," *IEEE Transactions on Geoscience and Remote Sensing*, vol. 60, pp. 1–12, 2022.
9. P. Zulch, M. Wicks, B. Moran, S. Suvorova, and J. Byrnes, "A new complementary waveform technique for radar signals," in *Proceedings of the 2002 IEEE Radar Conference (IEEE Cat. No.02CH37322)*, pp. 35–40, 2002.
10. Z. Matousek, J. Perdoch, M. Páček, S. Gazovová, and J. Ochodnický, "Radar signal waveform based on costas and walsh-hadamard codes as electronic counter-countermeasure," *IET Radar, Sonar & Navigation*, vol. 17, no. 6, pp. 1023–1039, 2023.
11. D. Kedia, M. Duhan, and S. Maskara, "Evaluation of correlation properties of orthogonal spreading codes for CDMA wireless mobile communication," in *2010 IEEE 2nd International Advance Computing Conference (IACC)*, pp. 325–330, 2010.
12. K. L. Gemba, H. J. Vazquez, J. Fialkowski, G. F. Edelmann, M. A. Dzieciuch, and W. S. Hodgkiss, "A performance comparison between m-sequences and linear frequency-modulated sweeps for the estimation of travel-time with a moving source," *The Journal of the Acoustical Society of America*, vol. 150, no. 4, pp. 2613–2623, 2021.

13. J. M. Velazquez-Gutierrez and C. Vargas-Rosales, "Sequence sets in wireless communication systems: A survey," *IEEE Communications Surveys & Tutorials*, vol. 19, no. 2, pp. 1225–1248, 2017.
14. D. Sarwate and M. Pursley, "Crosscorrelation properties of pseudorandom and related sequences," *Proceedings of the IEEE*, vol. 68, no. 5, pp. 593–619, 1980.
15. N. Touati, C. Tatkeu, A. Rivenq, C. Thierry, and Y. El Hillali, "Multi-user radar waveforms based on doubly coded costas signals," *IET Radar, Sonar & Navigation*, vol. 11, no. 2, pp. 277–284, 2017.
16. M. Jamil, H.-J. Zepernick, and M. I. Pettersson, "Performance assessment of polyphase pulse compression codes," in *2008 IEEE 10th International Symposium on Spread Spectrum Techniques and Applications*, pp. 166–172, 2008.
17. P. Ya-li and Y. Jin, "Chaos based orthogonal discrete frequency coding waveform design," in *2013 IEEE China Summit and International Conference on Signal and Information Processing*, pp. 30–33, 2013.
18. K. Rajwar, K. Deep, and S. Das, "An exhaustive review of the metaheuristic algorithms for search and optimization: taxonomy, applications, and open challenges," *Artificial Intelligence Review*, vol. 56, no. 11, pp. 13187–13257, 2023.
19. W. Chen, Z. Cai, R. Chen, and Z. Zhao, "Optimizing polyphase sequences for orthogonal netted radar systems," *Journal of Systems Engineering and Electronics*, vol. 23, no. 4, pp. 529–535, 2012.
20. H. Deng, "Polyphase code design for orthogonal netted radar systems," *IEEE Transactions on Signal Processing*, vol. 52, no. 11, pp. 3126–3135, 2004.
21. H. Khan, Y. Zhang, C. Ji, C. Stevens, D. Edwards, and D. O'Brien, "Optimizing polyphase sequences for orthogonal netted radar," *IEEE Signal Processing Letters*, vol. 13, no. 10, pp. 589–592, 2006.
22. L. Yunfo, L. Yuanyuan, W. Liqiang, and Z. Qi, "A multi-objective orthogonal waveform optimization method for MIMO radar," in *IET International Radar Conference 2015*, pp. 1–5, 2015.
23. Q. Sun, Y. Wang, Y. Li, and C. Tang, "Polyphase orthogonal waveform design for MIMO radar based on improved HHO algorithm," in *2022 IEEE 5th International Conference on Electronic Information and Communication Technology (ICEICT)*, pp. 804–807, 2022.
24. H. Deng, "Discrete frequency-coding waveform design for netted radar systems," *IEEE Signal Processing Letters*, vol. 11, no. 2, pp. 179–182, 2004.
25. W. Mehany, L. Jiao, and K. Hussien, "Orthogonal discrete frequency-coding waveform design based on modified genetic algorithm for MIMO-SAR," in *2014 9th IEEE Conference on Industrial Electronics and Applications*, pp. 1082–1086, June 2014.
26. L. Wang, F. Gao, J. Xu, D. Wang, M. He, and J. Yuan, "Orthogonal wideband hybrid-coding radar waveforms design," *Signal, Image and Video Processing*, vol. 11, pp. 103–111, Jan. 2017.
27. X. Luo, L. Guo, D. Song, S. Shang, and X. Li, "The research of orthogonal waveform design for ambiguity feature based on distributed MIMO radar," in *2021 6th International Conference on Communication, Image and Signal Processing (CCISP)*, pp. 425–429, 2021.
28. Y. Li, Y. Zhou, X. Li, J. Wang, Y. Wang, L. Fan, and F.-Y. Wang, "Unimodular complete complementary sequence with optimal trade-off between auto- and cross-ambiguity functions for MIMO radars," *IEEE Transactions on Intelligent Vehicles*, pp. 1–11, 2024.
29. D.-H. Kim, H.-J. Kim, and J.-H. Lim, "Design of optimized coded LFM waveform for spectrum shared radar system," *Sensors (Basel, Switzerland)*, vol. 21, no. 17, p. 5796, 2021.
30. H. He, P. Stoica, and J. Li, "Designing unimodular sequence sets with good correlations—including an application to MIMO radar," *IEEE Transactions on Signal Processing*, vol. 57, no. 11, pp. 4391–4405, 2009.
31. L. Xu, H. Liu, Q. Li, S. Zhou, and L. Hong, "Distributed MIMO radar orthogonal waveforms and mismatched filters design with expanded mainlobe," in *2016 CIE International Conference on Radar (RADAR)*, pp. 1–5, 2016.
32. Z. Huang, B. Tang, and S. Zhang, "Sequential optimisation of orthogonal waveforms for MIMO radar," *The Journal of Engineering*, vol. 2019, no. 21, pp. 7912–7917, 2019.
33. Y. Bu, J. Yang, X. Yu, Y. Xu, G. Cui, and Z. Jiang, "Fast optimization for unimodular sequences design with good correlation properties," in *2020 IEEE Radar Conference (RadarConf20)*, pp. 1–6, 2020.
34. H. Zebardast, M. Farhang, and A. Sheikhi, "Minimum PSL sequence set design for MIMO radars via manifold-based optimization," *IEEE Sensors Journal*, pp. 1–1, 2024.
35. Y. Chen, Z. Chen, Y. Zhang, J. Yang, and D. Li, "Joint design of doppler resilient unimodular discrete phase sequence waveform and receiving filter for multichannel radar," *IEEE Transactions on Signal Processing*, vol. 72, pp. 4207–4221, 2024.
36. M. He, Y. Jia, M. Sabrina Greco, F. Gini, and W.-Q. Wang, "Transmit Waveform Design Based on Ambiguity Function Shaping for Distributed Coherent Aperture Radar in MIMO Mode," *IEEE Geoscience and Remote Sensing Letters*, vol. 21, pp. 1–5, 2024.
37. J. Song, P. Babu, and D. P. Palomar, "Sequence set design with good correlation properties via majorization-minimization," *IEEE Transactions on Signal Processing*, vol. 64, no. 11, pp. 2866–2879, 2016.
38. H. He, P. Stoica, and J. Li, "On synthesizing cross ambiguity functions," in *2011 IEEE International Conference on Acoustics, Speech and Signal Processing (ICASSP)*, pp. 3536–3539, 2011.

39. M. Soltanalian and P. Stoica, "Designing unimodular codes via quadratic optimization," *IEEE Transactions on Signal Processing*, vol. 62, no. 5, pp. 1221–1234, 2014.
40. M. A. Richards, *Fundamentals of Radar Signal Processing*. McGraw-Hill Companies, Inc., 2005.
41. G. San Antonio, D. R. Fuhrmann, and F. C. Robey, "MIMO radar ambiguity functions," *IEEE Journal of Selected Topics in Signal Processing*, vol. 1, no. 1, pp. 167–177, 2007.
42. M. Alae-Kerahroodi, P. Babu, M. Soltanalian, and M. R. B. Shankar, *Signal Design for Modern Radar Systems*. Artech House, 2023.
43. M. Soltanalian and P. Stoica, "MERIT: A monotonically error-bound improving technique for unimodular quadratic programming," in *2014 IEEE International Conference on Acoustics, Speech and Signal Processing (ICASSP)*, pp. 5656–5660, 2014.
44. A. Martínez and J. L. Marchand, "SAR Image Quality Assessment," *Revista de Teledetección*, Nov. 1993.
45. N. Touati, C. Tatkeu, T. Chonavel, and A. Rivenq, "Design and performances evaluation of new Costas-based radar waveforms with pulse coding diversity," *IET Radar, Sonar & Navigation*, vol. 10, no. 5, pp. 877–891, 2016.